Physics of Fluids

Statistical analysis of temperature distribution on vortex surfaces in hypersonic turbulent boundary layer

Cite as: Phys. Fluids **31**, 106101 (2019); https://doi.org/10.1063/1.5115541
Submitted: 21 June 2019 . Accepted: 11 September 2019 . Published Online: 01 October 2019

Xin Li (李欣), Fu-Lin Tong (童福林), Chang-Ping Yu (于长平), and Xin-Liang Li (李新亮)

Physics of Fluids ARTICLE scitation.org/journal/phf

Statistical analysis of temperature distribution on vortex surfaces in hypersonic turbulent boundary layer

Cite as: Phys. Fluids 31, 106101 (2019); doi: 10.1063/1.5115541
Submitted: 21 June 2019 • Accepted: 11 September 2019 •
Published Online: 1 October 2019

Xin Li (李欣),[1,2] Fu-Lin Tong (童福林),[1,3] Chang-Ping Yu (于长平),[1] and Xin-Liang Li (李新亮)[1,2,a)]

AFFILIATIONS

[1]LHD, Institute of Mechanics, Chinese Academy of Sciences, Beijing 100190, China
[2]School of Engineering Science, University of Chinese Academy of Sciences, Beijing 100049, China
[3]Computational Aerodynamics Institute of China Aerodynamics Research and Development Center, Mianyang 621000, China

[a)]**Electronic mail:** lixl@imech.ac.cn

ABSTRACT

The nonuniform temperature distribution (NUTD) on the coherent vortex surfaces of hypersonic turbulent boundary layer (TBL) is studied using the conditional sampling technique. The direct numerical simulation data of Mach 8 flat-plate TBL flows with different wall temperatures, T_w/T_∞ = 10.03 and 1.9, are used for this research, and the coherent vortex surface is identified by the Ω-criterion. Two characteristic sides of the vortex are defined, which are represented by the positive and negative streamwise velocity fluctuations ($\pm u'$) of the vortex surfaces. The conditional sampling results between the mean temperature of the two sides show that there is a significant difference of up to 20% at the same wall-normal location. Furthermore, the velocity-temperature fluctuation correlations ($R_{u'T'}$ and $R_{v'T'}$) at the characteristic sides of vortex surfaces are studied. It is found that the temperature fluctuations are redistributed by the vortex rotational motion that has taken effect through $R_{u'T'}$ and $R_{v'T'}$ and then lead to the NUTD. The NUTD features are changed quantitatively by wall cooling but share the similar mechanism as that of the higher-temperature case.

I. INTRODUCTION

Turbulent boundary layers (TBLs) appear widely on hypersonic vehicles, and their fundamental mechanisms still need further clarification. One of the important aspects of TBL is vortex,[1,2] which plays an important role in the turbulent self-sustained mechanism with its rotational motion convecting fluid momentum and energy between the inner and outer layers. Therefore, the understanding of the features of vortices, such as their generation, structures, and propagation,[3] has been an enduring goal of research. Nevertheless, with high Mach numbers, these vortex features are affected by rapidly changing temperatures and their fluctuations because of the more complex coupling of the velocity and temperature fields. It is therefore necessary to study the correlations among velocities, temperatures, and vortex-related behaviors.

A number of experimental and numerical studies have been conducted on vortices at low and medium Mach numbers[4–8] and at high Mach numbers,[9,10] and some studies have considered wall temperature effects.[2,11,12] Consequently, many characteristics of vortices under various free incoming conditions have been effectively revealed. Most of the previous results relating to vortices focused on their rolling strength,[6] convection velocity,[13] dip angle,[14,15] and criterion.[16–20] However, studies of temperature distribution on vortex surfaces are still scarce.[21]

In this study, we use the direct numerical simulation (DNS) database with Ma_∞ = 8 established by Liang[22] to investigate the nonuniform temperature distribution (NUTD) on vortex surfaces under the conditions of wall temperature close to adiabatic wall and strong cold wall (TH and TL cases, respectively). The Ω-criterion, proposed by Liu,[23] is adopted to identify the vortices. Conditional sampling quadrant analysis on vortex surfaces and correlations between the velocity and temperature fluctuations are adopted to verify the NUTD and to reveal the paths of action. The results show that the maximum differences of NUTD are

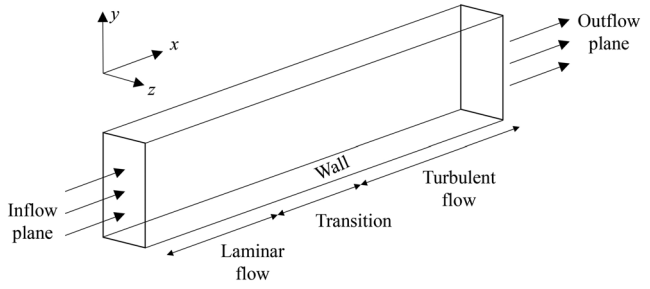

FIG. 1. Sketch of the computational domain and the coordinate system for current flat-plate flows, including laminar, transitional, and turbulent regions.

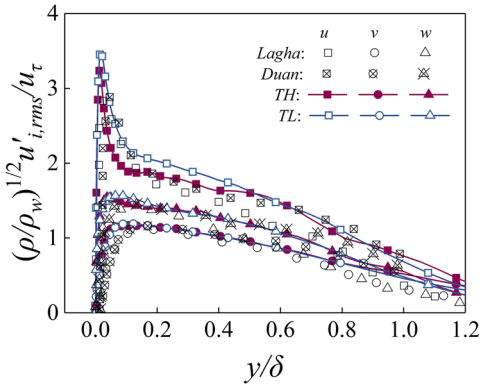

FIG. 2. Profiles of density-weighted turbulence intensities of three velocity fluctuation components. The hollow symbols are from the work of Lagha[10] with Ma_∞ = 2.5, and symbols with crosses represent the adiabatic results of Duan.[9]

20% between the $\pm u'$ sides of vortex surfaces for both temperature cases. The NUTD is induced by u' and v' in the dominated quadrant events, which enhance the corresponding temperature fluctuations and then speed up or delay the surface temperature changes through $R_{u'T'}$ and $R_{v'T'}$. The wall cooling keeps the crossing point of the mean temperatures on the $\pm u'$ sides far from the wall but maintains the same fundamental influence mechanism for the NUTD.

II. COMPUTATIONAL SETUP

A sketch of the computational domain and coordinate system of flat-plate flows is shown in Fig. 1. The x, y, and z are the streamwise, wall-normal, and spanwise directions, respectively. Table I summarizes the flow conditions, where Ma_∞ and T_∞ denote the free stream Mach number and temperature, respectively. The isothermal conditions are used at the wall in both cases. The wall-to-free-stream temperature ratio T_w/T_∞ is 10.03 and 1.9, respectively. $Re_{\delta 2}$, Re_θ, and Re_∞ are different definitions of the Reynolds numbers, where $Re_{\delta 2} = \rho_\infty U_\infty \theta/\mu_w$, $Re_\theta = \rho_\delta u_\delta \theta/\mu_\delta$, and $Re_\infty = \rho_\infty u_\infty l_\infty/\mu_\infty$. The table also gives the momentum thickness θ and boundary-layer thickness δ. In TBL flow, the recovery temperature is $T_r \equiv T_\infty[1 + (\gamma - 1)/2]Ma_\infty^2 r$ with r = 0.89. The computational domain size nondimensionalized by *inch* is taken as $L_x \times L_y \times L_z = 37 \times 0.7 \times 0.3$ for the TH case and $11 \times 0.7 \times 0.18$ for the TL case. The mesh numbers are $N_x \times N_y \times N_z = 12\,460 \times 100 \times 320$ and $8950 \times 90 \times 640$, and the corresponding mesh spacings in wall units are $dx^+ \times dy^+ \times dz^+ = 12.2 \times 0.96 \times 4.6$ and $11.2 \times 1.0 \times 4.5$ for the TH and TL cases, respectively. The snapshots of the y–z plane are collected at constant time intervals of $0.02\delta/U_\infty$ for TH and $0.04\delta/U_\infty$ for TL. The snapshot numbers are 1100 and 1800 for TH and TL, respectively.

III. RESULTS AND DISCUSSIONS

A. Velocity fluctuations and NUTD

Figure 2 plots the density-weighted root-mean-square (rms) of the velocity fluctuations across the boundary layers. When Morkovin's scaling, i.e., the variation in the mean flow properties, is taken into account, the turbulence intensities for both the cases and the previous results collapse greatly. This is an indication of the validity of the present computations.

The Ω-criterion is defined as the ratio of the vortical vorticity to the total vorticity. The practical criterion is expressed as

$$\Omega \approx \frac{b}{a + b + \varepsilon}, \tag{1}$$

and Ω = 0.52 is better chosen to define the vortex boundary.[23] This means that when the vorticity overcomes the deformation, denoted by a and b, respectively, the vortex is generated. Here,

$$a = \mathrm{trace}(A^T A) = \sum_{i=1}^{3}\sum_{j=1}^{3}(A_{ij}^2),$$

$$b = \mathrm{trace}(B^T B) = \sum_{i=1}^{3}\sum_{j=1}^{3}(B_{ij}^2),$$

where A is the symmetric part of the velocity gradient tensor and B is the antisymmetric part. The elements in A and B are given by $A_{ij} = \frac{1}{2}\left(\frac{\partial u_i}{\partial x_j} + \frac{\partial u_j}{\partial x_i}\right)$ and $B_{ij} = \frac{1}{2}\left(\frac{\partial u_i}{\partial x_j} - \frac{\partial u_j}{\partial x_i}\right)$, respectively. ε is a small number depending on the length and the velocity dimension. Recently, ε was determined as $\varepsilon = 0.001(b - a)_{max}$, in which

TABLE I. Computational conditions and grid parameters for the present DNS.

Case	Ma_∞	T_∞ (K)	T_w/T_∞	T_w/T_r	$Re_{\delta 2}$	Re_θ	Re_∞	θ	δ
TH	8	169.44	10.03	0.80	6328.23	3.71×10^4	5×10^6	7.41×10^{-3}	0.25
TL	8	169.44	1.9	0.15	6763.45	1.24×10^4	2×10^6	6.26×10^{-3}	0.12

$(b - a)_{max}$ is a fixed parameter at each time step in each case.[24,25] Compared with the Q-criterion and λ_2 method, the Ω-criterion has a clear physical meaning for vortex identification and an ability to extract a wide range of scales of vortices in the flow field. $\Omega = 0.52$ is selected, and the ε expression above is chosen as the maximum value among all the sampling time steps for the current vortex identification.

Figures 3(a) and 3(b) show parts of three-dimensional views of vortices and streak structures in fully developed turbulent regions. It can be observed that the vortices are more organized and less chaotic with lower vortex surface temperature in the TL case, which is similar to the results of previous study.[7] In the present compressible turbulence with high free stream Mach numbers, few integrated hairpinlike vortices exist in the flow fields, whereas most of the vortices have shapes conforming to canonical hairpins. The vortices are more likely to form on the low-speed streaks.[27,28] Figures 3(a) and 3(b) show that the large-scale broken vortices in the outer layer and the fine-scale streamwise vortices in the near-wall region are clearly identified by the Ω-criterion, which provides steady coherent structures for further analysis.

Figure 3(c) plots the bottom views of isosurfaces of coherent vortices colored by local instantaneous temperature. Longitudinal streamwise vortices arrange at the inner layer of the TBL, and their rotational motions dominate the behaviors of near-wall turbulence. It can be seen from the two inset figures that the NUTD occurs on every vortex and even in different parts of the same vortex. The former is observed by the comparison between the outer green vortices and inner yellow and red ones. The latter is visualized by the temperature changes on the surface of a single vortex. Previous studies on incompressible turbulence mentioned that the NUTD appears on upstream and downstream of vortex surfaces owing to their rotational motions.[21] However, as shown in Fig. 3(c), the upstream and downstream might not be adopted simply to identify the temperature distribution. Thus, it is necessary to find a more reasonable distribution on vortex surfaces.

Here, quadrant analysis, which is an effective method to measure the contribution of the Reynolds shear stress (RSS) and to study the turbulent bursting motion, should be considered to depict the vortex rotational motions. In quadrant analysis, four quadrants are created by streamwise and wall-normal velocity fluctuations, and the instantaneous RSS located in these quadrants are called four events, namely, (I) $Q1$, $u' > 0$, $v' > 0$; (II) $Q2$, $u' < 0$, $v' > 0$; (III) $Q3$, $u' < 0$, $v' < 0$; and (IV) $Q4$, $u' > 0$, $v' < 0$. As Corino and Brodkey[29] visualized, $Q2$ denotes the ejection event, that is, the low-speed streaks near the wall rise and break up under the action of rolling vortex pairs. $Q4$ is the sweep event, which means that the high-speed fluids in the outer layer sweep down to fill the space left by the near-wall fluid. $Q1$ and $Q3$ are called outward and inward interactions, which relate to the high-speed outer layer flow and low-speed inner layer flow, respectively.[30] Low-speed streaks are accompanied by higher temperature resulting from stronger stagnation velocities, and high-speed streaks are accompanied by the lower temperature. It is reasonable to combine $Q1$ and $Q4$ as a high-temperature part and $Q2$ and $Q3$ as a low-temperature part. These two parts of vortex surfaces are denoted as the $\pm u'$ sides, which are then used for further conditional sampling to represent the temperature distribution.

The Ω-criterion with threshold $\Omega = 0.52$ is adopted to identify the vortex surfaces in the snapshots of the selected y–z plane. Because the vortices pass through the y–z plane continuously, the vortex surfaces in this location can be extracted. The conditional

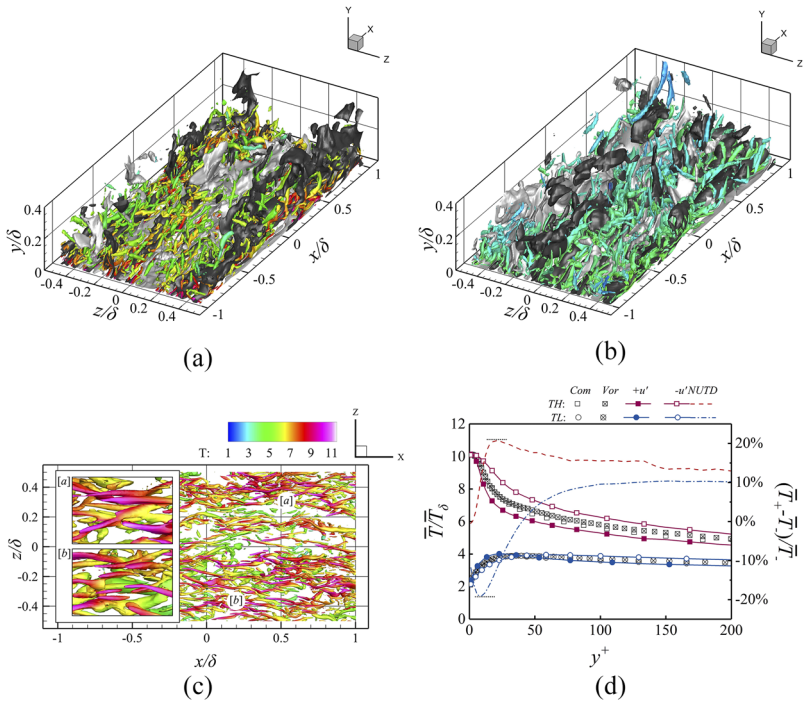

FIG. 3. NUTD on vortex surfaces. (a) TH and (b) TL. Three-dimensional views of coherent structures. Isosurfaces of vortices are colored with local instantaneous temperature. Isosurfaces of positive and negative streamwise velocity fluctuations are shown in white ($u'/u_\infty = 0.1$) and black ($u'/u_\infty = -0.1$), respectively. (c) The bottom view of (a). The two insert figures are the partial enlarged views of (a) and (b). (d) Different kinds of mean temperature distributions.

sampling technique is performed using the data points on the vortex surfaces and those related to the $\pm u'$ sides. Figure 3(d) compares several mean temperatures $\tilde{T}$ in the inner region, where the upper limit is at the lower part of logarithmic region of the mean velocity profile. Each $\tilde{T}$ is normalized by the boundary-layer edge mean temperature $\tilde{T}_\delta$. The nonsample results of the selected y–z planes are denoted by "*com*," the results sampled on the vortex surfaces at the selected y–z plane are denoted by "*vor*," and those sampled on the $\pm u'$ sides of the vortex surfaces are represented by the subscripts "+" and "−," respectively. The lines of $\tilde{T}_{TH,com}$ almost overlap with $\tilde{T}_{TH,vor}$ for both two cases. $\tilde{T}_+$ and $\tilde{T}_-$ are placed on both sides of $\tilde{T}_{com}$ and $\tilde{T}_{vor}$. These results exhibit that $\tilde{T}_{TH,-}$ is higher than $\tilde{T}_{TH,+}$ in almost the whole inner region, except for lower than $y^+ \leqslant 5$. The same trend of $\tilde{T}_{TL,-}$ occurs in approximately $y^+ \geqslant 40$, and the mean temperature alternation appears in $y^+ \leqslant 40$.

To quantify the NUTD on the $\pm u'$ vortex sides, a ratio is defined as $(\tilde{T}_+ - \tilde{T}_-)/\tilde{T}_-$, containing both positive and negative values. It is shown in Fig. 3(d) that the absolute maxima of NUTD are up to 20% at $y^+ \approx 25$ for the TH case and $y^+ \approx 15$ for the TL case. Far from the wall, the NUTDs tend to 10%, indicating that the NUTDs on the vortices become stable.

B. Reynolds shear stress distribution

Figures 4(a) and 4(b) plot the total RSS in the four quadrants. The sampled quadrant events show that both the ejection and sweep events near the wall are enhanced by cooling the wall. Additionally, ejection is stronger than sweeping in the wall-normal direction because under the effects of wall cooling, the larger probabilities of the small-scale velocity fluctuations for ejection increase more significantly than those for sweeping.[31] When sampled only on the vortex surfaces, quadrant events exhibit different behaviors. Especially in the TL case, the $Q2$ and $Q4$ motions alter their trends and become similar to those in the TH case. This indicates that when only the flows on the vortex surfaces are considered, the wall-cooling effects on the quadrant events are changed essentially. These phenomena can be understood as follows. As shown in Fig. 3, high-speed and low-speed streaks provide extra velocity fluctuations contributing to the whole quadrant events, as well as the strong rotational flows inside the vortex surfaces. However, these extra fluctuations may not be directly related to the vortex surface temperature, and we assume that the rotational motions on vortex surfaces dominate the NUTD, rather than the surrounding flow motions.

In order to demonstrate the weak correlation between the extra fluctuations and the NUTD, we sum the quadrant events based on the $\pm u'$ sides mentioned above; that is, $Q_+ = Q1 + Q4$ and $Q_- = Q2 + Q3$. As shown in the enlarged detail of Fig. 4, the complete sampled $\pm u'$ events exhibit two cross points in the near-wall region for both TH and TL, which is more complicated than the lines of the surface temperature distribution. This indicates that the quadrant events sampled on the whole flows cannot represent the immediate causes corresponding to the NUTD. While sampled on vortex surfaces, the $-u'$ event of TH is always stronger than the $+u'$ event for TH, and $\pm u'$ events for TL only have a cross point at $y^+ \approx 20$, which coincides well with the NUTD. Therefore, it is evident from these results that the $\pm u'$ events are the main reasons for the NUTD. The differences in quadrant event contributions between the complete flow field and vortex surfaces almost fluctuate between ±50%, which,

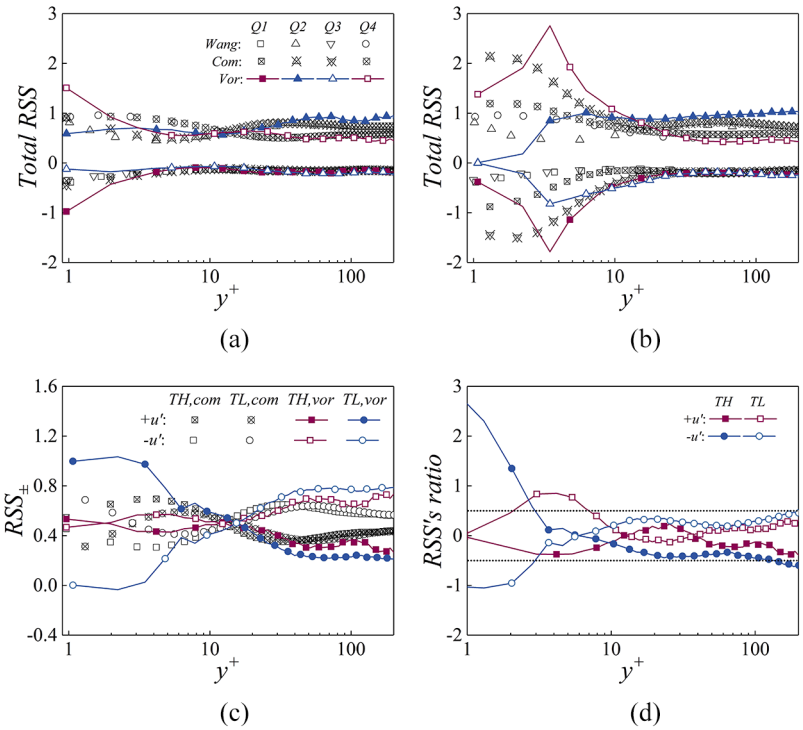

FIG. 4. Reynolds shear stress distributions. [(a) and (b)] Total RSS in four quadrants for TH and TL, respectively, compared with the results of Wang.[26] (c) RSS on the $\pm u'$ sides. (d) Differences between RSS of complete flows and the results sampled on the $\pm u'$ sides.

even for the TL case, increase to 260%, as shown in Fig. 4(d). This is the origin of prediction error of quadrant sampling on complete flow fields.

C. Velocity-temperature correlation

The manner in which the $\pm u'$ events work on the NUTD can be further analyzed by the instantaneous streamwise velocity fluctuations, namely, the near-wall streaks, and the correlation between the velocity and temperature fluctuations $-R_{u'T'}$, $R_{v'T'}$. As shown in Fig. 5, the streaks are selected at $y^+ \approx 15$, where the largest production term of the turbulent kinetic energy occurs.[32] These streaks are treated as the imprints left by the passing vortices at the buffer and low-law regions.[33,34] For the TH case, the velocity and temperature streaks are positively correlated at the near-wall region with shorter and more fragmentary shapes. For the TL case, the streaks become anticorrelated and more longitudinal in the streamwise direction. These results agree with those reported in previous research.[7]

In addition, Figs. 5(c) and 5(d) quantitatively plot $-R_{u'T'}$ and $R_{v'T'}$ in the near-wall region. $-R_{u'T'}$ and $R_{v'T'}$ sampled on whole sections for the TH case increase quickly from wall with the points of $-R_{u'T'} = 0$ and $R_{v'T'} = 0$ extremely close to the wall and then reach the peak values 0.6 and 0.4, respectively, which are similar to the DNS results with Ma_∞ up to 12.[9] This indicates that $-R_{u'T'}$ and $R_{v'T'}$ also have moderate correlations for hypersonic compressible TBLs with adiabatic wall. For the TL case, the peak values of $-R_{u'T'}$ and $R_{v'T'}$ decrease to 0.5 and 0.3, respectively, because of the higher inner compressibility effects caused by wall cooling. Additionally, the crossover locations of $R_{u'T'} = 0$ and $R_{v'T'} = 0$ shift further from the wall. At approximately $y^+ \leqslant 40$, $-R_{u'T'}$ and $R_{v'T'}$ show anticorrelations between the velocity and temperature fluctuations.

If sampled on vortex surfaces, $-R_{u'T'}$ and $R_{v'T'}$ for both the TH and TL cases nearly overlap with those sampled in the whole sections. Furthermore, the correlation coefficients on the $\pm u'$ sides are located on both sides of those for the whole flows, as well as the crossover points of the $\pm u'$ events, where $-R_{u'T'} = 0$ and $R_{v'T'} = 0$, as shown in the enlarged figures. Because these correlations are closely related to the effectiveness of the Morkovin's hypothesis,[35] the differences in the correlations on the $\pm u'$ sides are probably due to the different failure degrees of the Morkovin's hypothesis on vortex surfaces.

The mechanism can be explained as follows. Combined with the $\pm u'$ events plotted in Fig. 4, the $\pm u'$ events affect the NUTD through $-R_{u'T'}$ and $R_{v'T'}$. For TL, considering the $-R_{u'T'}$ on the vortex surfaces at lower y^+, the $+u'$ event dominates the fluctuations that represent the vortex rotational motions. Because of $-R_{u'T'} < 0$, $+u'$ corresponds to $+T'$ and vice versa. Thus, $+T'$ accelerates the vortex surface temperature in the small range of the correlation, and then, $\tilde{T}$ on the $+u'$ side reaches the peak value earlier. Meanwhile, $-T'$ slows down the increase in the surface temperature with the large range of the correlation, and then, the peak value of $\tilde{T}$ is delayed on the $-u'$ side. At larger y^+, according to the quadrant analysis, $+u'$ corresponding to $-T'$ is weaker than $-u'$. Additionally, the correlation level of $-u'$ is higher than that of $+u'$, which leads to $+T'$ accelerating $\tilde{T}$, as reflected by the $\tilde{T}$ line on the $-u'$ side moving up. $-T'$ slows down the increase in $\tilde{T}$ and then generates a crossing point at approximately $y^+ \approx 40$. These trends are consistent with the NUTD. For the TH case, the role of $-R_{u'T'}$ is the same as that in the TL case. However, because $-R_{u'T'} = 0$ is closer to the wall, there is no intersection for NUTD based on the $\pm u'$ events in the TH case.

Another mechanism of the NUTD is associated with $R_{v'T'}$. Figure 4(b) shows that at lower y^+ for the TL case, sweep events dominate on the vortex surfaces. That is, the strength of the statistical $+v'$ is lower than $-v'$. $R_{v'T'}$ remains anticorrelated from the wall to approximately $y^+ = 40$, meaning that $+v'$ corresponds to $-T'$ and vice versa. The position of $R_{v'T'} = 0$ on the $+u'$ side gets closer than that on the $-u'$ side. Therefore, $+T'$ on the $+u'$ side contributes to the surface temperature reaching its peak value. At $y^+ > 40$, the velocity

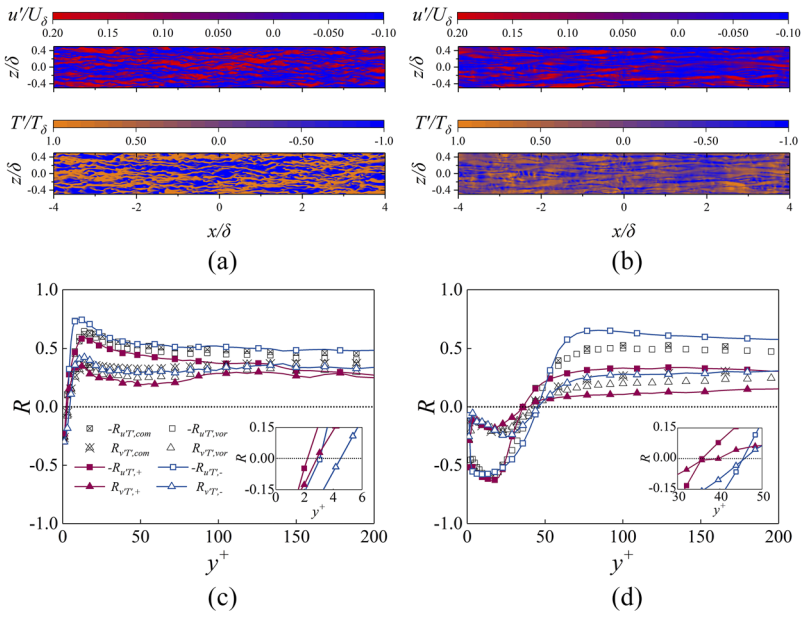

FIG. 5. Velocity and temperature streaks, and their quantitative correlations. [(a) and (c)] TH case and [(b) and (d)] TL case.

fluctuations on the vortex surfaces are dominated by ejection events, which indicates that the $+v'$ event is stronger than $-v'$. Because $R_{v'T'} > 0$, $+v'$ corresponds to $+T'$ and vice versa. $R_{v'T'}$ on the $-u'$ side is weaker than that on the $+u'$ side. This indicates that $\bar{T}$ is enhanced as $+T'$ increases, which leads to $\bar{T}$ on the $-u'$ side being higher than that on the $+u'$ side.

IV. CONCLUSIONS

To conclude, in order to investigate the NUTD on vortex surfaces, we perform global quadrant analysis, sampling quadrant analysis on vortex surfaces, and global and sampling correlation analysis on flat-plate TBLs with high and low wall temperature ($Ma_\infty = 8$). The Ω-criterion is adopted to identify the vortex surfaces.

The DNS results show that the organization of coherent vortices is enhanced through the increase in the Reynolds stress anisotropy under cooling wall condition. It is confirmed that the surface temperatures on the $\pm u'$ sides of vortices under high and low wall temperature conditions are not the same. The maximum differences in the temperatures on the $\pm u'$ sides reach approximately 20% near the wall and then decrease to approximately 10% far from the wall.

It is seen that the sampling quadrant events on vortex surfaces are consistent with the NUTD for both the TH and TL cases, which avoid the influence of other coherent structures, such as high-speed and low-speed streaks, and are the more proximate causes leading to the NUTD.

In the manner of working on $-R_{u'T'}$ and $R_{v'T'}$, T' on the vortex surfaces are changed by the conditional sampling quadrant events. A stronger $+u'$ event enhances $+T'$ on the $+u'$ side near the wall, and then $+T'$ accelerates the increase in $\bar{T}$. On the contrary, far away from the wall, the dominant $-u'$ event increases $+T'$ on the $-u'$ side, thus increasing $\bar{T}$. This mechanism is qualitatively similar between high and low wall temperatures but enhanced in the TL case represented by the zero-crossing points of the quadrant analyses and correlations far away from the wall. We suppose that the correlation differences on the $\pm u'$ sides are due to the different failure degrees of Morkovin's hypothesis on vortex surfaces.

ACKNOWLEDGMENTS

This work was supported by the NSFC Project (Grant Nos. 91852203 and 11472278), the National Key Research and Development Program of China (Grant No. 2016YFA0401200), the Science Challenge Project (Grant No. TZ2016001), and the Strategic Priority Research Program of Chinese Academy of Sciences (Grant Nos. XDA17030100 and XDC01000000). The authors thank the National Supercomputer Center in Tianjin (NSCC-TJ) and the National Supercomputer Center in Guangzhou (NSCC-GZ) for providing computer time.

REFERENCES

[1] S. K. Robinson, "Coherent motions in the turbulent boundary layer," Annu. Rev. Fluid Mech. **23**, 601–639 (1991).
[2] Y. B. Chu, Y. Q. Zhuang, and X. Y. Lu, "Effect of wall temperature on hypersonic turbulent boundary layer," J. Turbul. **14**, 37–57 (2013).
[3] W. Schoppa and F. Hussain, "Coherent structure generation in near-wall turbulence," J. Fluid Mech. **453**, 57–108 (2002).
[4] T. Maeder, N. A. Adams, and L. Kleiser, "Direct simulation of turbulent supersonic boundary layers by an extended temporal approach," J. Fluid Mech. **429**, 187–216 (2001).
[5] S. Pirozzoli, F. Grasso, and T. B. Gatski, "Direct numerical simulation and analysis of a spatially evolving supersonic turbulent boundary layer at m=2.25," Phys. Fluids **16**, 530–545 (2004).
[6] S. Pirozzoli, M. Bernardini, and F. Grasso, "Characterization of coherent vortical structures in a supersonic turbulent boundary layer," J. Fluid Mech. **613**, 205–231 (2008).
[7] L. Duan, I. Beekman, and M. P. Martin, "Direct numerical simulation of hypersonic turbulent boundary layers. Part 2. Effect of wall temperature," J. Fluid Mech. **655**, 419–445 (2010).
[8] M. Lagha, J. Kim, J. D. Eldredge, and X. L. Zhong, "Near-wall dynamics of compressible boundary layers," Phys. Fluids **23**, 065109 (2011).
[9] L. Duan, I. Beekman, and M. P. Martin, "Direct numerical simulation of hypersonic turbulent boundary layers. Part 3. Effect of Mach number," J. Fluid Mech. **672**, 245–267 (2011).
[10] M. Lagha, J. Kim, J. D. Eldredge, and X. L. Zhong, "A numerical study of compressible turbulent boundary layers," Phys. Fluids **23**, 015106 (2011).
[11] A. Trettel and J. Larsson, "Mean velocity scaling for compressible wall turbulence with heat transfer," Phys. Fluids **28**, 026102 (2016).
[12] C. Zhang, L. Duan, and M. M. Meelan, "Effect of wall cooling on boundary-layer-induced pressure fluctuations at Mach 6," J. Fluid Mech. **822**, 5–30 (2017).
[13] E. F. Spina, A. J. Smits, and S. K. Robinson, "The physics of supersonic turbulent boundary layers," Annu. Rev. Fluid Mech. **26**, 287–319 (1994).
[14] Q. C. Wang, Z. G. Wang, and Y. X. Zhao, "An experimental investigation of the supersonic turbulent boundary layer subjected to concave curvature," Phys. Fluids **28**, 096104 (2016).
[15] S. C. Deng, C. Pan, J. J. Wang, and G. S. He, "On the spatial organization of hairpin packets in a turbulent boundary layer at low-to-moderate Reynolds number," J. Fluid Mech. **844**, 635–668 (2018).
[16] V. Kolar and J. Sistek, "Corotational and compressibility aspects leading to a modification of the vortex-identification Q-criterion," AIAA J. **53**, 2406–2410 (2015).
[17] J. H. Elsas and L. Moriconi, "Vortex identification from local properties of the vorticity field," Phys. Fluids **29**, 015101 (2017).
[18] J. Yao and F. Hussain, "Toward vortex identification based on local pressure-minimum criterion in compressible and variable density flows," J. Fluid Mech. **850**, 5–17 (2018).
[19] J. M. Liu, Y. S. Gao, and C. Q. Liu, "An objective version of the rortex vector for vortex identification," Phys. Fluids **31**, 065112 (2019).
[20] H. Chen, Z. H. Wang, and J. Z. Wang, "Evaluation of vortex identification methods based on two- and three-dimensional swirling strengths," Phys. Fluids **30**, 125102 (2018).
[21] Z. Hui, A. Y. Wei, K. Luo, and J. R. Fan, "Direct numerical simulation of turbulent boundary layer with heat transfer," Int. J. Heat Mass Transfer **99**, 10–19 (2016).
[22] X. Liang and X. L. Li, "Direct numerical simulation on Mach number and wall temperature effects in the turbulent flows of flat-plate boundary layer," Commun. Comput. Phys. **17**, 189–212 (2015).
[23] C. Q. Liu, Y. Q. Wang, Z. W. Duan, and Y. D. Yang, "New Omega vortex identification method," Sci. China: Phys., Mech. Astron. **59**(8), 684–711 (2016).
[24] X. R. Dong, Y. Q. Wang, X. P. Chen, Y. L. Dong, Y. N. Zhang, and C. Q. Liu, "Determination of epsilon for Omega vortex identification method," J. Hydrodyn. **30**, 541–548 (2018).
[25] Y. N. Zhang, X. Y. Wang, Y. N. Zhang, and C. Q. Liu, "Comparisons and analyses of vortex identification between Omega method and Q criterion," J. Hydrodyn. **31**, 224–230 (2019).
[26] L. Wang and X. Y. Lu, "Statistical analysis of coherent vortical structures in a supersonic turbulent boundary layer," Chin. Phys. Lett. **28**, 034703 (2011).
[27] R. J. Adrian, C. D. Meinhart, and C. D. Tomkins, "Vortex organization in the outer region of the turbulent boundary layer," J. Fluid Mech. **422**, 1–54 (2000).

[28]S. Pirozzoli and M. Bernardini, "Turbulence in supersonic boundary layers at moderate Reynolds number," J. Fluid Mech. **688**, 120–168 (2011).
[29]E. R. Corino and R. S. Brodkey, "A visualization of the wall region in turbulent flow," J. Fluid Mech. **37**, 1–30 (1969).
[30]J. M. Wallace, "Quadrant analysis in turbulence research: History and evolution," Annu. Rev. Fluid Mech. **48**(1), 131–158 (2016).
[31]X. Li, C. P. Yu, and X. L. Li, "Wall temperature effects on the Reynold stress of flat-plate turbulent boundary layer: A numerical investigation," Adv. Appl. Math. Mech. **11**, 653–663 (2019).
[32]C. Bauer, D. Feldmann, and C. Wagner, "On the convergence and scaling of highorder statistical moments in turbulent pipe flow using direct numerical simulations," Phys. Fluids **29**, 125105 (2017).
[33]J. Jimenez, "Coherent structures in wall-bounded turbulence," J. Fluid Mech. **842**, P1 (2018).
[34]A. Shekar and M. D. Graham, "Exact coherent states with hairpin-like vortex structure in channel flow," J. Fluid Mech. **849**, 76–89 (2018).
[35]L. Duan, I. Beekman, and M. P. Martin, "Direct numerical simulation of hypersonic turbulent boundary layers. Part 4. Effect of high enthalpy," J. Fluid Mech. **684**, 25–59 (2011).